



ÉCOLE CENTRALE LYON

UE FLE – TC3  
FLUIDS AND ENERGY  
EXPERIMENTAL AND NUMERICAL STUDIES

---

## Planes and Fluid Forces

---

***Students :***

Neirouz BOUCHAIRA  
Sylvain CROSNIER  
Iris DELMAS  
David WAGNER

***Theme 12 :***  
FLUID FORCES AND  
STRUCTURE

March 2024

---

**Abstract** — Characterizing the forces acting on an aircraft is essential in order to obtain optimal operation, for example by consuming as little fuel as possible. The stall angle of the wing profile studied was evaluated at  $12^\circ$  and characterizes the angle from which lift is no longer ensured. The experiment was able to highlight the importance of using flaps in the takeoff phase in order to increase lift and their nuisance in hovering flight. The optimal operating point of the wing angle of incidence is between  $1^\circ$  and  $6^\circ$ .

The plotting of the pressure contours around a profiled body made it possible to note where the overpressure zones were located and therefore to deduce the point of application of the lift which occurs at the leading edge when it faces the flow. The opposite is observed for turbine blades that are turned back relative to the wing.

The wake created by a profiled body could be highlighted by measuring the total pressure downstream of a blade and by plotting the contour of the air speed on the simulation of the wing profile carried out.

The thrust measurements carried out during the tests on turbojets highlighted the direct relationship between fuel flow rates and the thrust generated. A comparison between theoretical and experimental thrust values revealed a slight overestimation of the theoretical calculations.

**Keywords:** Lift, Drag, Airfoil, Static pressure, Thrust force

---

# Contents

<b>1</b>	<b>Introduction</b>	<b>1</b>
<b>2</b>	<b>Theoretical reminders</b>	<b>1</b>
2.1	Profiled body . . . . .	1
2.2	Similitude . . . . .	2
2.3	Turbojet . . . . .	2
<b>3</b>	<b>Experimental installations used</b>	<b>4</b>
3.1	Wind tunnel . . . . .	4
3.2	Blade grid . . . . .	4
3.3	Turboreacteur . . . . .	5
<b>4</b>	<b>Instrumentation</b>	<b>6</b>
4.1	Pitot tube . . . . .	6
4.2	3-point Pitot probe . . . . .	6
4.3	Static pressure tapings . . . . .	7
4.4	Aerodynamic balance with strain gauge . . . . .	7
4.5	Water manometer . . . . .	7
<b>5</b>	<b>Experiments performed and results</b>	<b>7</b>
5.1	Saturation of coefficients . . . . .	7
5.2	Lift and drag coefficients for the wing and the blade . . . . .	8
5.3	Comparison with a numerical model: wing profile . . . . .	10
5.4	Static pressure distribution around the wing and the blade . . . . .	11
5.5	Wake downstream of the blade grid . . . . .	13
5.6	Thrust force of a turbojet . . . . .	14
<b>6</b>	<b>Conclusion</b>	<b>15</b>
<b>A</b>	<b>Annexe</b>	<b>18</b>
A.1	Classic Pitot Tube [5] . . . . .	18
A.2	Saturation of coefficients . . . . .	18
A.3	Calculation of the density of air . . . . .	19
A.4	Calculation of Mach number . . . . .	19
A.5	Fluent Simulation . . . . .	20
A.6	Other figures . . . . .	22
A.7	Programs <i>Matlab</i> used . . . . .	23

## Notations

- $Re$  : Reynolds number of the flow  
 $L$  : Lift force norm [N]  
 $D$  : Drag force norm [N]  
 $F$  : Resultant of the lift force and the drag force [N]  
 $C_L$  : Lift coefficient  
 $C_D$  : Drag coefficient  
 $\rho$  : Density of the studied fluid [ $\text{kg m}^{-3}$ ]  
 $S$  : Surface area of the studied profiled body [ $\text{m}^2$ ]  
 $\alpha$  : Incidence of the profiled body [rad]  
 $p_i$  : Static pressure at point  $i$  [Pa]  
 $q$  : Dynamic pressure [Pa]  
 $U_\infty$  : Fluid velocity far upstream of the system [ $\text{m s}^{-1}$ ]  
 $U$  : Fluid velocity [ $\text{m s}^{-1}$ ]  
 $\dot{m}$  : Fluid mass flow rate [ $\text{kg s}^{-1}$ ]  
 $A$  : Turbojet outlet section [ $\text{m}^2$ ]  
 $\nu$  : Kinematic viscosity of the fluid studied [ $\text{m}^2 \text{s}^{-1}$ ]  
 $c$  : Specific heat capacity of air [ $\text{J K}^{-1} \text{kg}^{-1}$ ]

# 1 Introduction

The aeronautics sector has always been among the most innovative. Over the years, engineers have been able to use their knowledge to further optimize the efficiency of machines and their performance. In this sense, studying the forces exerted on the wings or within the reactor of an aircraft is essential if we want to obtain optimal operation.

For an aircraft to fly, it is necessary to ensure several points. First, to move forward, the thrust of the jets must at least compensate for the friction of the air on the fuselage of the aircraft, also called drag. Second, to take off, the lift of the aircraft must be high enough to compensate for the effects of gravity. Finally, it will be interesting to study the airflow and its geometry in the vicinity of a turbine blade in order to deduce the pressure force exerted on the latter.

Here are the main forces exerted on an aircraft and which will be studied in this report. We will focus on characterizing them by studying a wing profile in a wind tunnel, an airflow on a blade grid and finally the operation of a turbojet similar to those used on aircraft.

## 2 Theoretical reminders

### 2.1 Profiled body

An aerodynamic profile is characterized by a vertical force or lift force  $\mathbf{L}$  greater than the horizontal force or drag force  $\mathbf{D}$ . This criterion is therefore important for an aircraft wing whose profile is shown schematically in figure 1, as well as its flap.

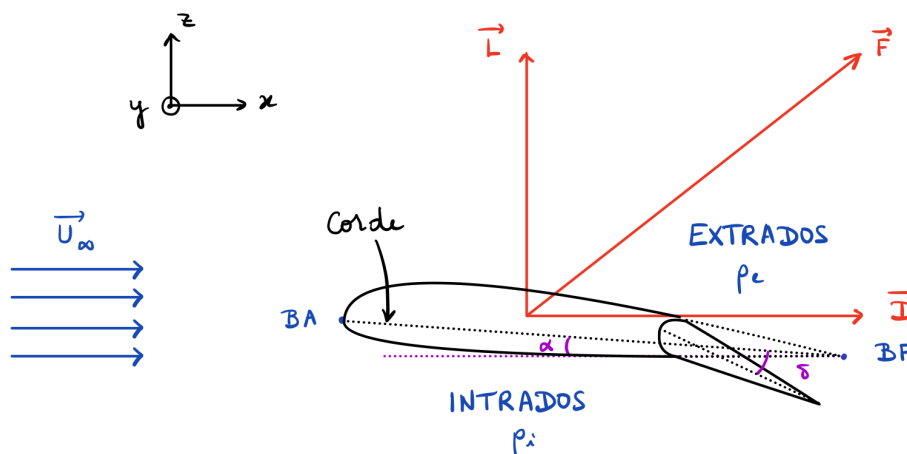


Figure 1: Diagram of a wing profile with the notations used.

The leading edge BA: leading edge is the one facing the flow. The chord connects the leading edge to the trailing edge BF. We denote  $p_e$  as the pressure on the upper surface and  $p_i$  as the pressure on the lower surface. Furthermore,  $\alpha$  is defined as the angle of inclination of the chord relative to the  $Ox$  axis and  $\delta$  is the angle between the flap and the chord. Finally,  $U_\infty$  is the flow speed upstream of the wing.

To generate lift, it is necessary to obtain an overpressure at the lower surface:  $p_i > p_e$ . Indeed, the pressure forces will therefore be greater on the lower surface than on the upper surface, which will allow the aircraft to be lifted. The total pressure force generated by a dynamic profile is expressed by:

$$\mathbf{F} = - \int_S p \mathbf{n} dS \quad (1)$$

where  $S$  is the surface of the profiled body and  $\mathbf{n}$  the normal vector to this surface. The objective will therefore be to characterize  $\mathbf{L}$  and  $\mathbf{D}$  as a function of  $\alpha$  and  $\delta$  for the wing in particular.

## 2.2 Similitude

To be able to apply the results obtained on the model to a real aircraft, two types of similarities must be respected:

- Geometric similarity: the geometry of the wing profile in the wind tunnel must be the same as the geometry of the real wing.
- Dynamic similarity: the same dimensionless numbers characterize the model and reality.

We will therefore consider the dimensionless lift coefficients  $C_L$  and drag coefficients  $C_D$  associated respectively with the forces  $\mathbf{L}$  and  $\mathbf{D}$ :

$$C_L = \frac{L}{\frac{1}{2}\rho U_\infty^2 S} \quad C_D = \frac{D}{\frac{1}{2}\rho U_\infty^2 S} \quad (2)$$

where  $S$  is the surface area of the wing, i.e. the product of its chord by its length, respectively 10 cm and 30 cm for the wind tunnel experiment.

## 2.3 Turbojet

*In this section, equations including shutdown parameters and static parameters (e.g. shutdown (or total) pressure and static pressure) will be presented. Shutdown values will be indexed by a 0. The index 5 indicates that the values considered are those at the outlet of the jet engine nozzle (figure 2).*

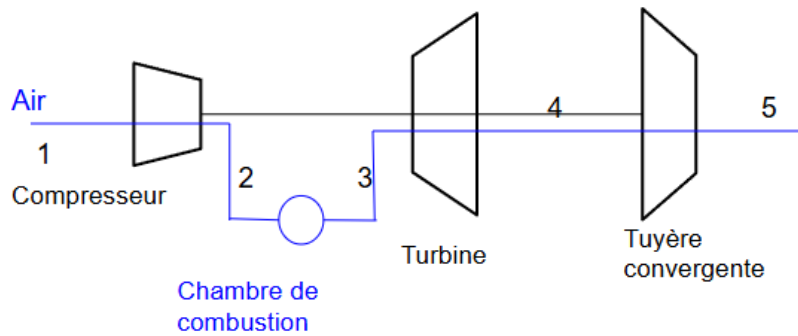


Figure 2: Diagram of the different elements constituting the turbojet engine as well as the positions of the measurement points used during the experiment (original French figure)

**Obtaining the outlet speed**  $U_5$  is by definition the shutdown temperature [1]:

$$U_5 = \sqrt{2c(T_{05} - T_5)} \quad (3)$$

where  $c$  is the specific heat capacity of the air. Now, still by definition of the stopping variables and in static mode:

$$T_5 = T_{05} \left( \frac{p_5}{p_{05}} \right)^{\frac{\gamma-1}{\gamma}} \quad (4)$$

$p_5$  is here the static pressure at the sensor 5 at the nozzle outlet. It is approximately equal to atmospheric pressure because the streamlines can be considered as being parallel at the outlet. We are therefore faced with a free jet which allows us to state that the static pressure is the atmospheric pressure at each point of the jet. The atmospheric pressure is measured using a mercury barometer. At the time of the experiment:  $p_{atm} = 747 \text{ mmHg} \approx 99\,600 \text{ Pa}$ .  $\gamma$  is an arithmetic mean of  $\gamma_g$  and  $\gamma_a$  (the respective adiabatic coefficients of the burnt gases and air) because the outgoing fluids are a mixture in equal proportions of air and burnt gases. This last hypothesis will be discussed later.

**Obtaining the outlet flow rate**  $\dot{m}_5$  can be easily expressed as a function of the outlet air density  $\rho$ , the outlet section  $A$  and finally the outlet velocity  $U_5$ :

$$\dot{m}_5 = \rho_5 A U_5 \quad (5)$$

The outlet diameter is 5.587 cm. Since the Mach number of the flow is  $M \sim 0.28$  (see section A.4 in the Appendix for the detailed calculation of the Mach number), the air can be considered compressible. Thus,  $\rho$  is not a constant of the flow and must be calculated at each location with the equation:

$$\rho_5 = \frac{p_5}{r T_5} \quad (6)$$

valid for ideal gases. At the outlet:  $r$  is an arithmetic mean of  $r_g$  and  $r_a$  because the outgoing fluids are in theory both air and burnt gases as mentioned previously.

## 3 Experimental installations used

### 3.1 Wind tunnel



Figure 3: Wind tunnel profile: complete experimental installation (*left*) and strain gauge balance (*right*)

To study the forces acting on aircraft wings, a wind tunnel was used (figure 3). It contains two NACA 4412 standard wing profiles. One is connected to a strain gauge balance while the second is equipped with static pressure taps all around its geometry (about 25 taps).

The wing connected to the balance allows to measure the lift and drag coefficients for different angles  $\alpha$  of the wing and  $\delta$  of the flap. The other profile allows to access the static pressure distribution around the studied body and thus to establish a link between the latter and the performance of the wing.

The two profiles are identical. They each have a chord of 10 cm and a span of 30 cm.

The wind tunnel can generate flows of speeds ranging from 0 to  $25\text{m s}^{-1}$ . This speed is measured upstream of the wing using a Pitot tube.

### 3.2 Blade grid

A blade grid is useful to study the geometry of a flow within a turbine. Within an aircraft, turbines can be found in various places such as:

- In the reactor. Indeed, turbojets rely on the principle of action-reaction (Newton's third law) by accelerating a mass of air which by reaction will create the thrust force [2]. Blades are also present on the fan which compresses the air entering the reactor.
- In the ECS (*Environmental Control System*) which regulates the temperature and pressure inside the aircraft for the crew and passengers [3]. Here, it expands the incoming hot air in order to reduce its temperature.

The installation used (figure 4) is composed of 10 blades installed periodically in space: the inter-blade distance is 10 cm. The system allows to model the blades of a turbine that would have been unfolded then flattened.



Figure 4: Study of a blade grid: experimental installation

The air flow is accelerated thanks to a convergent so as to be facing the blades. A potentiostat is used to vary the fan rotation speed and therefore the air speed [4].

A fixed-position Pitot tube is used to measure the dynamic pressure upstream of the blade grid. A 3-point hook-type Pitot probe, whose inclination can be modified, is placed close to the downstream of the grid. A second 3-point hook-type Pitot probe, whose inclination and vertical position can be measured, is placed far downstream. A blade equipped with 36 static pressure taps is used to obtain the static pressure profile on its surface.

### 3.3 Turboreacteur

Used as an engine on commercial airliners, turbojets are generally placed under the wings of an aircraft.



Figure 5: Turboreacteur used during the experiment

The mini laboratory "MiniLab™ Gas Turbine Power System" allows you to study a turbojet composed of a centrifugal compressor, a combustion chamber, a turbine and a

nozzle (figure 5) [1].

The compressor is embedded on the same shaft as the turbine that drives it in rotation. Compressed air is injected to trigger the rotation of the latter. The combustion chamber is supplied with kerosene.

This test bench provides access to measurements of:

- shutdown temperatures  $T_{0,1-5}$  (°C)
- total pressures  $p_{0,2-5}$  (PSI gauge)
- dynamic pressure  $q_1 = \frac{1}{2}\rho_1 V_1^2$  (PSI)
- engine speed
- inlet kerosene flow rate
- thrust force  $F_{exp}$

Numbers 1 to 5 correspond to the positions of the measurement points illustrated in the figure 2.

## 4 Instrumentation

### 4.1 Pitot tube

The Pitot tube [5] is a probe that measures the speed in a flow, by a pressure difference between two points. The probe must be aligned parallel and facing the average flow for the measurement to be optimal [6]. The theory underlying this tool is explained in Appendix section A.1.

### 4.2 3-point Pitot probe

When using a conventional Pitot probe, it is necessary to align the probe facing the flow to have the static pressure on the side of the probe and the total pressure at the tip of the probe. In the event of poor alignment, the values would be distorted. Thus, when the direction of the flow is not known, it is necessary to try to align the axis of the probe in this direction. To do this, there are Pitot probes with three pressure points (figure 6): a stopping point, a left static pressure point and a right static pressure point. The orientation of the probe is then modified until there is a zero pressure difference between the left and right static points: the probe is then aligned with the direction of the flow.

Furthermore, to have a measurement at the same point in space regardless of the angle of inclination of the 3-point pitot tube, the probe has a hook shape so that the pressure points are on its axis of rotation.



Figure 6: 3-inlet Pitot tube

### 4.3 Static pressure tappings

In order to measure the static pressure on a profiled body (wing or blade), sensors are regularly spaced on the wing. The direction of the hole is perpendicular to the surface of the wing. Thus, the sensor will not be sensitive to the dynamic pressure due to the flow of the fluid but only to the Brownian motion of the fluid molecules. This type of measurement then makes it possible to deduce by integration the pressure force on the profiled body.

One of the technologies used is the water manometer. These are small diameter tubes (of the order of cm) using the fundamental principle of fluid statics. They make it possible to find the pressure at a point thanks to the height of a column of water. These instruments will be interesting for tracing pressure contours on the profiled bodies studied.

### 4.4 Aerodynamic balance with strain gauge

To measure lift and drag, it is possible to use an aerodynamic balance with strain gauge. The balance of the wind tunnel bench (figure 3 on the right) has 3 components because it measures lift, drag and the moment that is not recorded during the experiment.

The principle is as follows: we measure the deformation of a blade under the effect of the component of the force considered. The use of Wheatstone bridges (classic electrical circuit) then makes it possible to measure a potential difference by knowing the mechanical characteristics of the deforming blade [7].

### 4.5 Water manometer

Water manometers are small diameter tubes (of the order of cm) using the principle of fluid statics. They make it possible to find the pressure at a point thanks to the height of a column of water. These instruments will be useful for plotting pressure contours on the profiled bodies studied. They will be used in particular to characterize the static pressure around the wing profile used.

## 5 Experiments performed and results

### 5.1 Saturation of coefficients

For the measurements performed on the experimental installation (wind tunnel or blade grid) to be usable on a full-size aircraft, the principle of similarity must be respected as presented in section 2.1. We will only present the dynamic similarity obtained for the wind tunnel experiment because the blade grid was not equipped with a strain gauge balance necessary for calculating  $C_L$  and  $C_D$ .

If the Reynolds number of the flow studied is calculated for the wind tunnel experiment (speed of the order of  $10 \text{ m s}^{-1}$  and air density of  $1.2 \text{ kg m}^{-3}$ ):

$$Re \sim \frac{1.2 \times 10 \times 10^{-1}}{10^{-5}} = 1.2 \times 10^5 \quad (7)$$

and compared to that which would be obtained for an airplane whose wings would have a chord of 1 m and a speed of  $100 \text{ m s}^{-1}$  ( $360 \text{ km h}^{-1}$ ):

$$Re \sim \frac{1.2 \times 100 \times 1}{10^{-5}} = 1.2 \times 10^7 \quad (8)$$

The dynamic viscosity of air is of the order of  $10^{-5}$  Pa s.

The dynamic similarity is therefore not respected. However, we show that for  $Re > 10^5$ ,  $C_L$  and  $C_D$  are independent of  $Re$ : there is saturation of the coefficients. This allows us to apply the wind tunnel results to a real case.

The angle of incidence of the wing  $\alpha$  as well as the incidence of the flap  $\delta$  is then set to  $0^\circ$  and the measurement of the lift and drag coefficients is carried out for different values of incident speeds  $U_\infty$ .

From each value of  $L$  and  $D$ , we must subtract their respective offsets, that is, the value provided by the aerodynamic balance at zero incident speed for each of these coefficients.

On the two characteristics obtained reported in the appendix A.2, we observe a saturation of the coefficients above a certain Reynolds number (therefore a certain speed). The number above which saturation occurs is  $Re \simeq 2 \times 10^5$  for both coefficients. The rest of the wind tunnel experiments will then be carried out at a speed higher than that corresponding to this Reynolds number of the order of  $25 \text{ m s}^{-1}$ .

## 5.2 Lift and drag coefficients for the wing and the blade

**Wing profile** The lift and drag forces acting on the wing by varying the wing angle of incidence  $\alpha$  and the flap angle  $\delta$  are measured using the aerodynamic balance. The results are reported in figures 7 and 8.

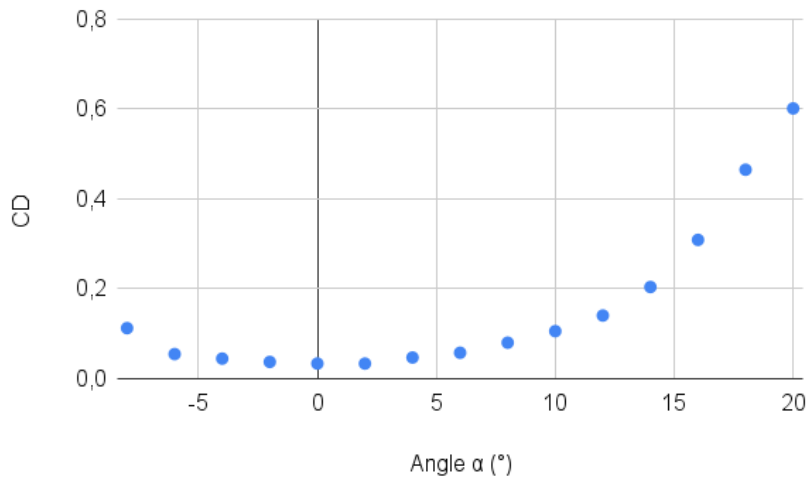


Figure 7: Lift coefficient  $C_L$  as a function of  $\alpha$  and  $\delta$

Figure 7 shows an increasing trend of the coefficient  $C_L$  up to  $\alpha = 12^\circ$  (linear up to  $\alpha = 10^\circ$ ). From this angle,  $C_L$  decreases. This is explained by the fact that the streamlines no longer follow the profile and therefore the condition  $p_e < p_i$  is no longer respected. There is a stall: this is the separation of the boundary layer. In addition, we note that when the angle of incidence of the flap  $\delta$  increases,  $C_L$  becomes more important. This variation in the flap angle is used during the takeoff phase to have more lift and therefore take off more easily.

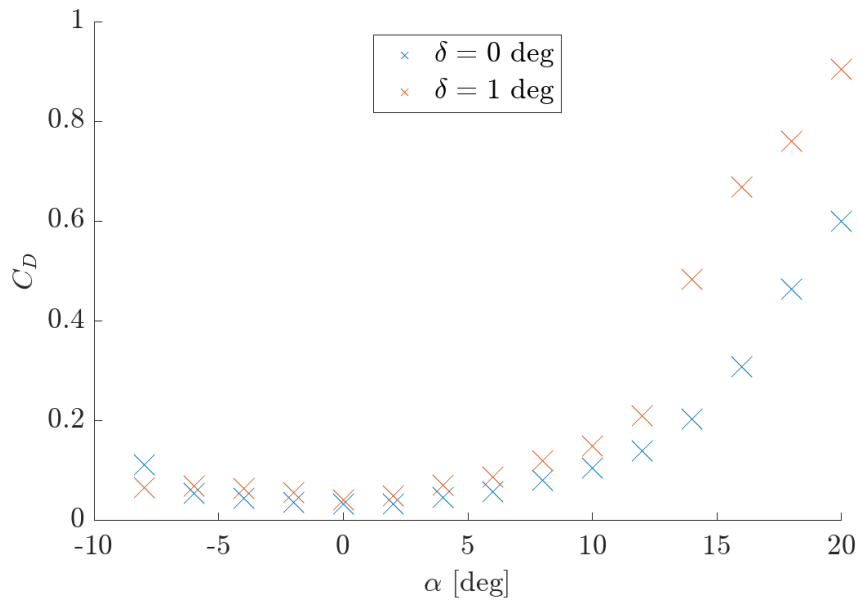


Figure 8: Drag coefficient  $C_D$  as a function of  $\alpha$  and  $\delta$

However, we can see in figure 8 that the drag coefficient  $C_D$  also increases with  $\delta$ , which seems consistent because the surface area perceived by the flow is larger, so friction increases. Using the flaps is therefore not useful throughout the flight. Indeed, since the aircraft’s cruising speed is higher, it is not necessary to have a high lift coefficient to stay in flight. It is therefore more interesting to try to minimize the drag coefficient in order to consume less fuel to generate the necessary thrust during a hovering flight.

The characteristic  $C_L/C_D$  as a function of  $\alpha$  (see figure 9) is important in aeronautics since it allows us to find the optimal operating point at cruising altitude. The objective is to obtain the highest possible lift while minimizing drag. The operating point is therefore the maximum of the plotted characteristic. Figure 9 shows that it is obtained for a wing incidence angle between  $1^\circ$  and  $6^\circ$ .

**Blade grid** Moreover, the program *Matlab* presented in the appendix A.7 allowed, thanks to the static pressure measurements, to integrate this pressure and to obtain the drag and lift forces. The results are summarized in the table 1. The dimensioning was done by taking  $S = 0.032 \text{ m}^2$  the product of the chord by the blade span.

	$C_L$	$C_D$
$U_\infty \sim 3 \text{ m s}^{-1}$	-0.022	0.0591
$U_\infty \sim 6 \text{ m s}^{-1}$	-0.469	1.2785

Table 1: Lift and drag coefficients for the blade

It is difficult to compare these values to the coefficients of the wing. Despite the fact that the Reynolds numbers of the two experiments are approximately the same, the geometric similarity is not respected at all.

We note that the lift is negative because the blade, unlike the wing, has its extrados oriented towards the ground (figure 20 in Appendix). When the air speed has doubled,

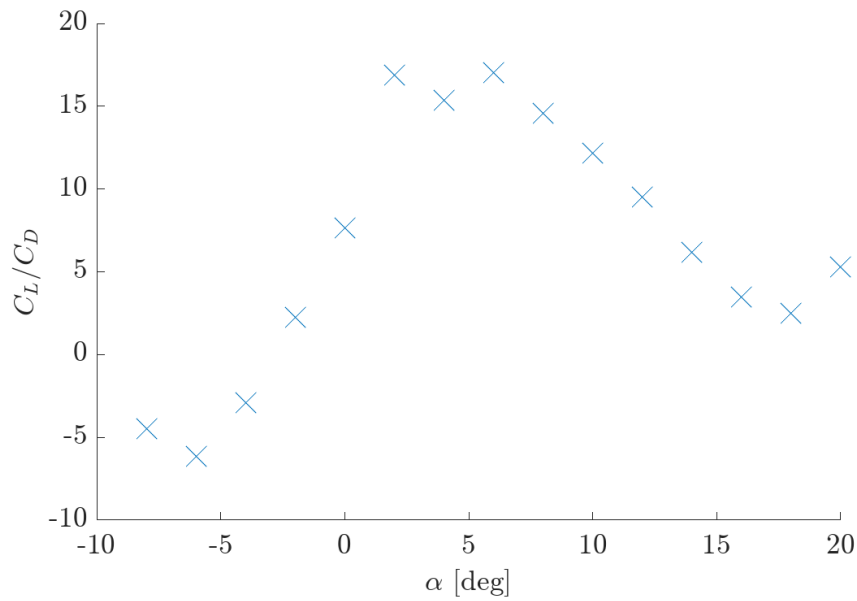


Figure 9: Characteristic  $C_L/C_D$  of the wing studied as a function of  $\alpha$  allowing to find the ideal operating point at cruising altitude

the lift coefficient also seems to have been multiplied by two while the drag has increased more drastically. This shows the predominance of turbulent effects leading to a strong loss of energy occurring at high turbine speeds. These losses are difficult to avoid since the speed of the turbine of an engine is imposed by the speed desired by the pilot of the aircraft.

### 5.3 Comparison with a numerical model: wing profile

A mesh representing a wing profile is modeled under *AnsysFluent* (appendix figure 16). The modeling allows to compare the experimental and numerical results as well as to access a greater number of data compared to the data collected in the wind tunnel.

The complete numerical protocol used for the simulation can be found in appendix A.5. The choice of the viscous Spalart-Allmaras model is quite frequent for aeronautical problems and in particular for flows around walls [8].

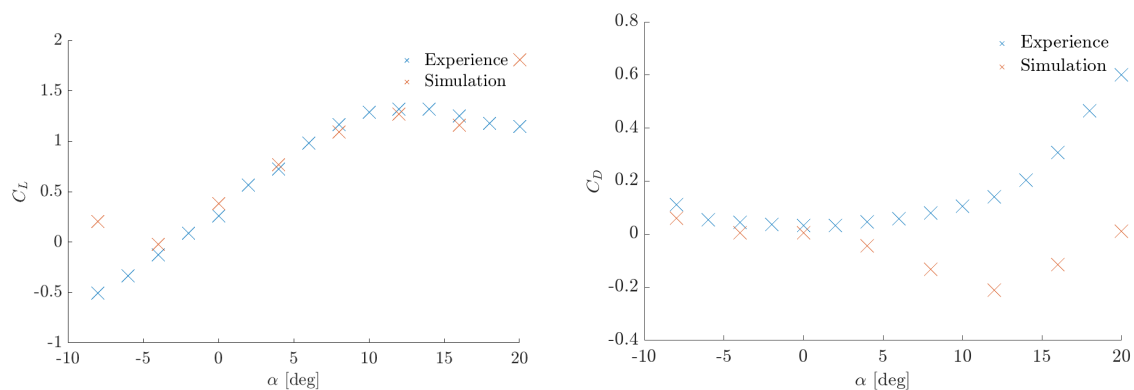


Figure 10: Comparison of drag and lift coefficients obtained numerically and experimentally

The results are quite satisfactory at low angles of incidence (figure 10). However, the values of  $C_D$  obtained by simulation are much lower than those calculated experimentally at high  $\alpha$ . This phenomenon can be explained in particular by the fact that *AnsysFluent* is a software that searches for stationary solutions. However, since the flow is turbulent and not stationary when the angles of incidence are high – the wing oscillated around an equilibrium position during the wind tunnel experiment – it is difficult to converge numerically towards a stable solution. This is also shown by the residuals which take rather high values even at the end of the simulation (Appendix figure 17).

The simulation made it possible to trace in particular the contour of the air speed in the vicinity of the wing (Appendix figure 18). This speed drops sharply directly downstream of the profile at low  $\alpha$  and over an increasingly large area as the angle increases. This phenomenon is due to the turbulence of the flow which produces a wake at the origin of the drag. This is why we observe an increase in  $C_D$  with  $\alpha$ .

## 5.4 Static pressure distribution around the wing and the blade

Drawing the static pressure contour around a profiled body can be interesting to try to improve its geometry in order to increase the coefficient  $C_L/C_D$ . More precisely, it will be the static pressure coefficient  $C_P$  as a function of the abscissa  $x$  at the profile level (see coordinate system on the diagram in figure 1) that will be interesting to study (principle of similarity). This coefficient is expressed with the formula:

$$C_P = \frac{p - p_{atm}}{\frac{1}{2}\rho U_\infty^2} \quad (9)$$

**Pressure contour on the wing profile** We therefore carry out a second experiment on the wing profile by measuring at  $\alpha = 0^\circ$  and  $\delta = 0^\circ$ , the pressure measured around the wing profile. The measurement is carried out using a water multi-manometer consisting of 25 static pressure taps, distributed over the profile as follows [9] :

- on the extrados:  $x$  (mm) = 0-2-4-6-8-10-13-16-20-30-40-50-60-70-80-90
- on the intrados:  $x$  (mm) = 2-4-6-8-10-20-30-40-50-60-70-85.

The figure 11 is obtained. It was decided to plot  $-C_P$  because a pressure drop is observed at the extrados, this therefore allows to obtain the values of the extrados at the top of the graph and those of the intrados at the bottom.

We observe that the pressure difference is greater at the leading edge than at the trailing edge. Thus the lift is mainly concentrated in this area. It is this part of the wing that will therefore undergo great mechanical stress. There is therefore not only work to optimize the wing profile but also structural choices to guarantee the strength of the wing and limit the weight of the aircraft. Nevertheless, pressure forces are not the only ones to intervene and we must also consider friction and a possible stall of the boundary layer that occurs for a certain angle of attack  $\alpha$ . A good compromise must be found between low wake and high pressure force.

**Static pressure contour around a blade** In comparison, figure 12 shows two dimensionless static pressure profiles on a blade for two different air inlet speeds in the blade

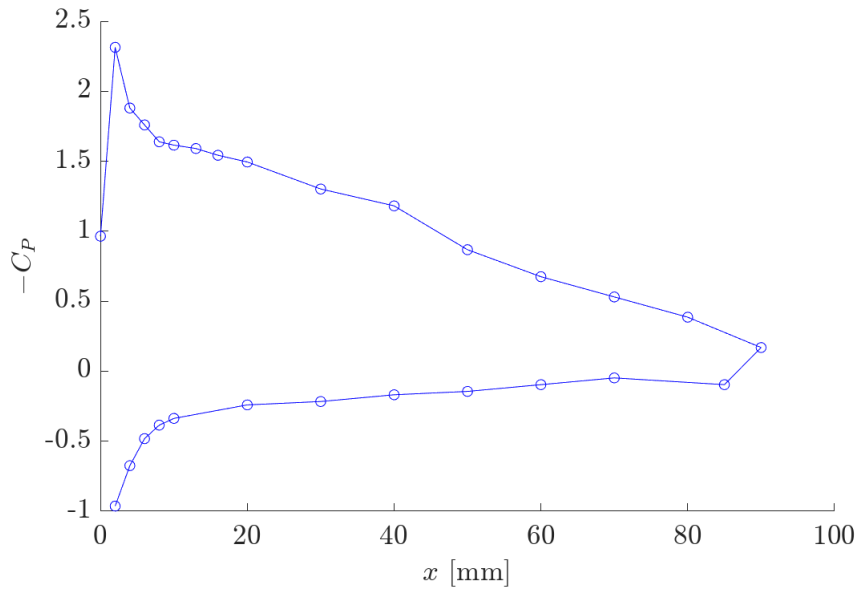


Figure 11: Evolution of the coefficient  $-C_P$  as a function of the measurement position  $x$

grid. In general, dimensionless is used to obtain unitary  $C_P$  on the leading edge of the blade:

$$C_P = \frac{p_{stat}^{blade} - p_{stat}^{\infty}}{\frac{1}{2}\rho U_{\infty}^2} \quad (10)$$

However, since the accuracy of the low-speed case is problematic, the upstream dynamics being low, a difference of 1 Pa can be largely amplified. To limit this effect, we take the downstream data of averaged speed:  $U_{aval}$ . The downstream dynamics being much higher, the measurement imprecision is minimized. We therefore choose:

$$C_P = \frac{p_{stat}^{aube} - p_{atm}}{\frac{1}{2}\rho U_{aval}^2} \quad (11)$$

We therefore observe the superposition of the two pressure profiles.

The major difference between these profiles and that of the wing lies in the angle of incidence of the blade which is high compared to that of the wing which was zero during this experiment. The geometry of the two profiled bodies is also very different and must be taken into account (figures 19 and 20 in Appendix).

The static pressure variations obtained can be explained through simple physical arguments. The fluid is accelerated on the extrados because of the reduction in section. Indeed, the reduction in static pressure induces an increase in the speed of the fluid because the total pressure remains constant. The pressure at the outlet is approximately equal to  $p_{atm}$ : we are indeed in the presence of a free jet.

A blade can therefore have two roles: either the driving fluid can exert its action on it (in the case of a wind turbine for example), or the blade can exert its action on the fluid. In the second case, the blade can be used to obtain the correct pressure gradient of the fluid, for example in the turbine of a turbojet. The rotating blades accelerate the fluid, then a static rectifier converts the acquired kinetic energy into static pressure. Thanks to a stack of rotor-stator stages, the pressure gradient in the turbine can be regulated. The same principle is used for a centrifugal compressor placed at the inlet of the reactor,

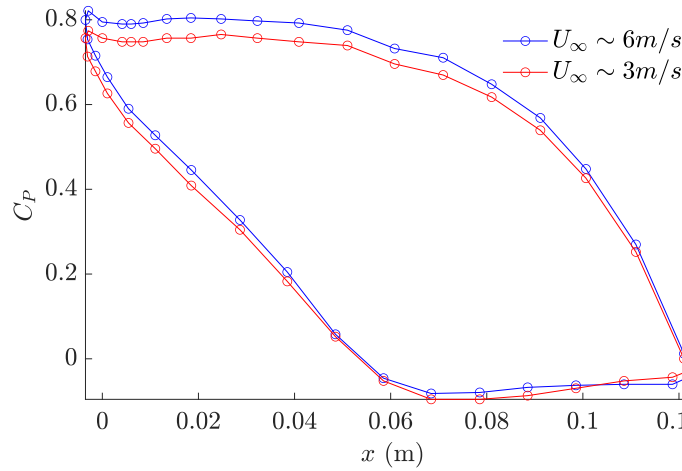


Figure 12: Adimensionalized profiles of static pressures on a blade for two values of fluid speed

except that the stator is a diffuser and not blades. However, in transient conditions, since the speed of the incoming fluid is low, aircraft engines are equipped with an electric motor that only operates during takeoff: the blades must be driven because the speed of the incoming fluid is not yet high enough. In the experiment carried out on the turbojet, compressed air is used to start the reactor.

### 5.5 Wake downstream of the blade grid

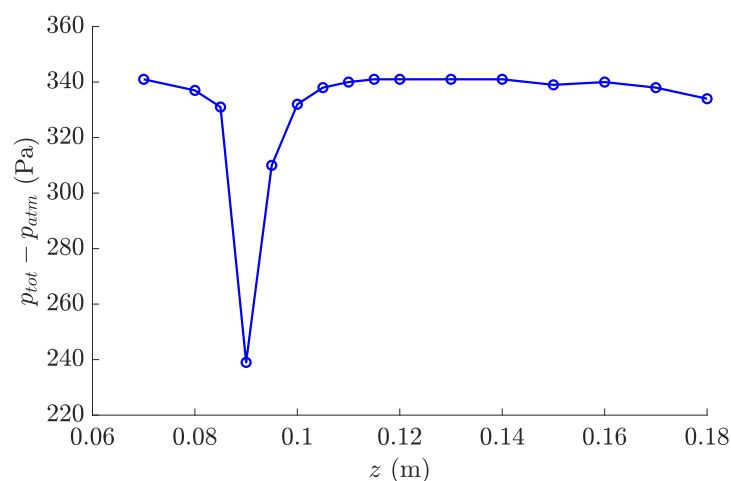


Figure 13: Total pressure downstream

Figure 13, represents the total pressure of the flow downstream of a blade at the center of the grid as a function of altitude  $z$  (see coordinate system figure 1). The measurements were made on an amplitude equal to the spatial period of the grid pattern.

We observe that the total pressure is almost constant and equal to the total pressure upstream, measured at the Pitot tube. This can be physically explained by Bernoulli's theorem. If we consider a streamline passing far from the blades, and the flow is stationary, non-viscous (because it is outside the boundary layer due to the blade), incompressible and without volume force, then there is conservation of the total pressure.

The pressure drop is due to the fact that the wake of the boundary layers of the intrados and extrados meet. As the speed drops abruptly at this level, the total pressure too. This phenomenon can be observed in figure 18 in the Appendix illustrating the air speed gradient around the simulated wing profile.

The objective of aerodynamics is therefore to reduce the wake area as much as possible because it is the one that is mainly responsible for the drag of the blade and therefore slows it down. The wake can also cause vibrations and damage mechanical parts. The challenge for the turbine of a turbojet is to lose as little energy as possible in friction because it is less energy to move the plane forward and therefore more fuel is consumed.

## 5.6 Thrust force of a turbojet

Wind tunnel experiments on the aircraft wing profile have highlighted the existence of a drag force that opposes the movement. It is therefore necessary to provide a force opposing the drag force so that the aircraft can move forward: this is the thrust force, which is provided by the aircraft's turbojet.

**Experimental protocol** The turbojet is operated for 3 different kerosene flow rates. The flow rate followed a sequence low, medium, high, medium, low to study the influence of the temperature of the elements on the measured values (the reactor is cold at the start and takes time to heat up).

Once the kerosene flow rate was set, a wait of a few minutes was necessary so that a steady state could be established. The reactor being connected to a computer software, all the data could be collected on a post-experiment USB key. The data sampling period is 3s which therefore requires a good analysis.

**Data filtering** An indicator that the steady state has been reached is the stabilization of the temperature at the nozzle outlet. The 5 steady states obtained can be observed figure 21 in the Appendix.

Drawing this graph made it possible to identify the steady state zones and therefore to know at what times the data collected during the experiment could be used. 5 times were selected. An average of the values on each step could have been considered in order to increase the accuracy of the results. This method was not implemented due to lack of time. The 5 times are: 14h52min42s; 14h54min47s; 14h57min54s; 14h59min39s and 15h01min55s.

**Data processing** The objective at the end of the processing is to be able to compare a theoretical value of the thrust force with an experimental value measured directly in the reactor as explained in section 3.3. This theoretical value is expressed as follows:

$$F_{the} = \dot{m}_5 U_5 \quad (12)$$

with  $\dot{m}_5$  the mass flow rate of the air at the nozzle outlet and  $U_5$  its speed at the same location. The expression found follows a balance of momentum on a control volume including the inlet and outlet of the reactor. The equations used to obtain  $\dot{m}_5$  and  $U_5$  were presented in the theoretical part section 2.3.

**Discussion of results** A *Matlab* code reported in the appendix (listing ??) allows to calculate the 5 theoretical values of the thrust which are compared to the values measured by the device (from which an offset present even when the reactor is off must be removed).

The values obtained are reported in table 2.

Kerosene flow (L h <sup>-1</sup> )	8.4769	12.5297	12.8989	12.3365	8.8846
$\dot{m}_5$ (kg s <sup>-1</sup> )	0.1544	0.2114	0.2189	0.2107	0.1662
$F_{the}$ (N)	22.5309	41.803	45.066	41.724	26.129
$F_{exp}$ (N)	19.3972	34.0197	37.481	34.796	22.919

Table 2: Theoretical and experimental values of thrust forces with a kerosene flow rate following the sequence: low, medium, high, medium, low

The temperature of the reactor elements does not have a great influence on the values. Indeed, similar values are observed for the forces measured whether the engine is hot or cold at equal flow rate.

In addition, the theory tends to slightly overestimate the values of the thrust forces which may come from the fact that the fluid does not contain an equal fraction of air and burnt gases as it was considered in the calculations. Nevertheless the order of magnitude remains the same and seems quite low. Indeed, one would expect a turbojet, even on a small scale, to produce a force greater than the weight of a mass of a few kilograms. Normally, the device used produces thrusts of the order of 90 N but several TPs have taken place since its last cleaning which may explain the difference.

These values show in all cases how difficult it is to generate significant thrust and that it requires a great deal of power to move an aircraft forward.

## 6 Conclusion

This project explored the fluid forces acting on an aircraft to optimize its performance. Based on experimental and numerical analyses, lift and drag forces on a wing airfoil, static pressure distribution around a wing and turbine blades, and the thrust force of a turbojet engine were studied in detail.

For the wing analysis, the critical stall angle for the studied profile was determined to be 12°. Lift can no longer be maintained for a higher angle. The use of flaps at takeoff increases lift considerably, but is not useful in cruising flight due to an increase in drag. The optimum wing angle of incidence, ensuring a maximum lift/drag ratio, is between 1° and 6°.

Thrust measurements performed during turbojet tests have highlighted the direct relationship between fuel flow rates and thrust generated. A comparison between theoretical and experimental thrust values revealed a slight overestimation of theoretical calculations.

This study highlights the importance of using control surfaces, such as flaps, for improving aircraft performance. The experimental and numerical methods used in this

framework constitute a robust tool for continuous optimization in the field of aeronautical engineering. One possible avenue of thought is the refinement of numerical models in order to better simulate turbulent and unsteady flows, as well as the extension of the analysis to a wider range of aerodynamic profiles with different geometries.

## References

- [1] *Fiche technique N°26 Turboreacteur*. Tech. rep. UE Fluides et Energie, Département MFAE, Ecole Centrale de Lyon - Moodle.
- [2] L'Avionnaire. *LES TURBOMACHINES*. Consulté le 19 juin 2024. URL: <https://www.lavionnaire.fr/MotorPrincipe.php>.
- [3] Wikipédia. *Environmental control system*. Consulté le 19 juin 2024. URL: [https://en.wikipedia.org/wiki/Environmental\\_control\\_system#:~:text=In%20aeronautics%2C%20an%20environmental%20control%20system%20%28ECS%29%20of%20,cooling%20of%20avionics%2C%20smoke%20detection%2C%20and%20fire%20suppression..](https://en.wikipedia.org/wiki/Environmental_control_system#:~:text=In%20aeronautics%2C%20an%20environmental%20control%20system%20%28ECS%29%20of%20,cooling%20of%20avionics%2C%20smoke%20detection%2C%20and%20fire%20suppression..)
- [4] *ANALYSE EXPERIMENTALE DE L'ÉCOULEMENT DANS UNE GRILLE D'AUBES PLANE DE TURBINE*. Tech. rep. UE Fluides et Energie, Département MFAE, Ecole Centrale de Lyon - Moodle.
- [5] *Étude d'un jet libre*. Tech. rep. Groupe C1b1<sub>2</sub> : N.Bouchaira, S.Crosnier, I.Delmas, T.Zaoui.
- [6] *Tube de Pitot*. Tech. rep. Ecole centrale de Lyon.
- [7] Onera. *Méthodes de mesure en aérodynamique*. URL: [https://www.onera.fr/sites/default/files/ressources\\_documentaires/cours-exposes-conf/cours-aerodynamique-mesures-efforts.pdf](https://www.onera.fr/sites/default/files/ressources_documentaires/cours-exposes-conf/cours-aerodynamique-mesures-efforts.pdf).
- [8] *Spalart-Allmaras turbulence model*. Consulté le 18 juin 2024. URL: [https://en.wikipedia.org/wiki/Spalart%E2%80%93Allmaras\\_turbulence\\_model](https://en.wikipedia.org/wiki/Spalart%E2%80%93Allmaras_turbulence_model).
- [9] *Fiche technique PROFIL EN SOUFFLERIE*. Tech. rep. Version du 07/12/2023. UE Fluides et Energie, Département MFAE, Ecole Centrale de Lyon - Moodle.
- [10] *NACA4412 Test Case*. Consulté le 17 juin 2024. URL: <https://www.cfdsupport.com/OpenFOAM-Training-by-CFD-Support/node381.html>.

## A Annexe

### A.1 Classic Pitot Tube [5]

The Pitot tube is a probe that measures the velocity in a flow, by a pressure difference between two points. The probe must be aligned with the mean flow, and oriented against the flow [6]. Figure 14 shows a diagram of this device:

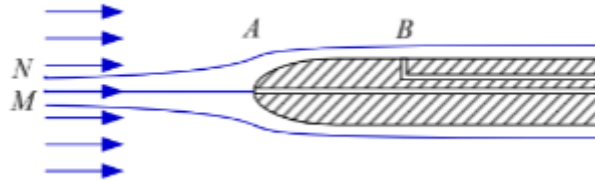


Figure 14: Schema of a Pitot Tube

Point A is called the stopping point, because there is a particular streamline that stops at this point, so  $U_A = 0$ .

A gas with a flow velocity less than  $100 \text{ m s}^{-1}$  is considered incompressible. The effect of gravity can be neglected given the small variation in height, in the absence of dissipative phenomena between M and A, Bernoulli's theorem gives the relation:

$$p_M + \rho \frac{U^2}{2} = p_A \quad (13)$$

The same theorem applied between N and B gives:

$$p_B + \rho \frac{U_B^2}{2} = p_N + \rho \frac{U_N^2}{2} \quad (14)$$

By making the approximations  $U_M = U_N = U_B$  and  $p_M = p_N$ , we obtain the relation:

$$p_A = p_B + \rho \frac{U_M^2}{2} \quad (15)$$

Hence the relationship allowing to measure the speed at point M from a pressure difference:

$$U_M = \sqrt{\frac{2(p_A - p_B)}{\rho}} \quad (16)$$

### A.2 Saturation of coefficients

For the measurements carried out on the experimental installation (wind tunnel or blade grid) to be usable on a full-size aircraft, the principle of similarity must be respected as mentioned in section 2.1.

In figures 15a and 15b, we observe that  $C_D$  and  $C_L$  become quite constant from  $Re \simeq 20000$  (maximum variations of 0.01 for  $C_L$  and 0.04 for  $C_D$ ). This implies that from the speed  $15.7 \text{ mmH}_2\text{O}$ , the two coefficients do not vary much. This then justifies the superposition of the results of figures 7 and 8 obtained at different speeds but higher than the threshold of  $15.7 \text{ mmH}_2\text{O}$ .

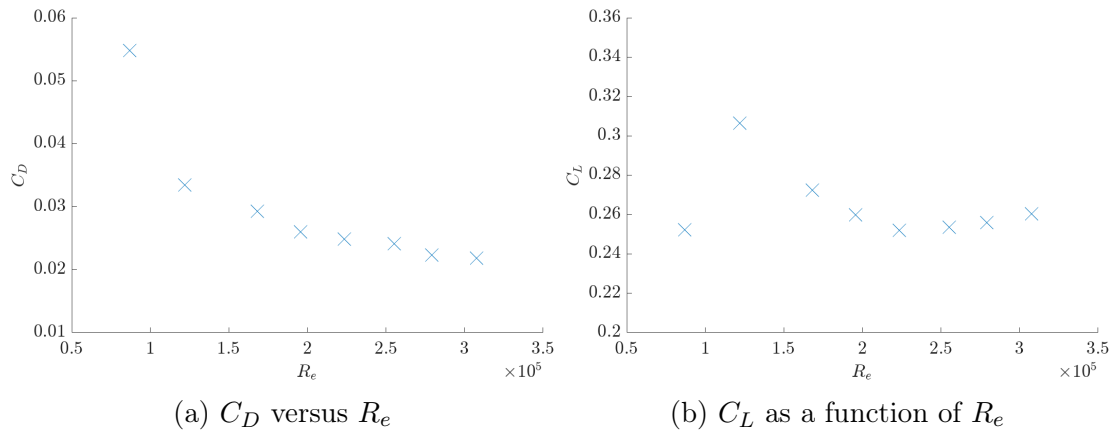


Figure 15: The coefficients of drag  $C_D$  and lift  $C_L$  as a function of the Reynolds number  $R_e$

### A.3 Calculation of the density of air

If we consider air as an ideal gas, its density can be written as:

$$\rho = \frac{MP}{RT} \quad (17)$$

with  $T$  the air temperature,  $M$  its molar mass,  $R$  the Ideal Gas constant and  $P$  the air pressure.

$P$  and  $T$  are measured using a mercury barometer.  $M$  is taken equal to  $28.965 \text{g mol}^{-1}$  for numerical applications.

### A.4 Calculation of Mach number

As a reminder:

$$M = \frac{U}{r\gamma T} \quad (18)$$

Let's calculate this number at the nozzle outlet.  $U_5 \sim 160 \text{m s}^{-1}$  (calculated via *Matlab*),  $\gamma = 1.4$ ,  $r = 286 \text{J K}^{-1} \text{kg}^{-1}$  and  $T_5 \sim 806 \text{K}$  (static temperature) which gives:  $M \sim 0.28$ .

### A.5 Fluent Simulation

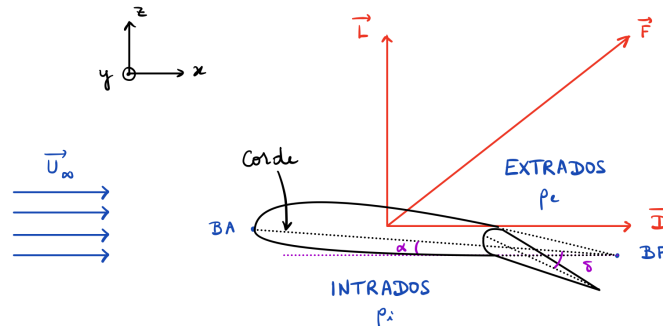


Figure 16: Mesh used for Fluent simulation

<b>Geometry and Mesh</b>	2D mesh of a wing profile with the same dimensions as the experimental profile
<b>Fluid and Properties</b>	Air: $\rho = 1.161\text{kg m}^{-3}$ and $\nu = 1.7894 \times 10^{-5}\text{m}^2 \text{s}^{-1}$
<b>Physical Model</b>	Viscous model: Spalart-Allmaras (classic for wing profiles)
<b>Boundary conditions</b>	<ul style="list-style-type: none"> <li>• Input: speed of norm 25.91 m/s and variable incidence</li> <li>• Output: Atmospheric pressure</li> <li>• Wing: adhesion</li> </ul>
<b>Time-space discretization</b>	Coupled scheme of order 2 in space + pseudo-transient.
<b>Quantity of interest</b>	Horizontal and vertical resultants of the pressure force on the wing
<b>Verification and Validation</b>	<ul style="list-style-type: none"> <li>• Verification: convergence of the residuals</li> <li>• Validation: comparison with experimental data</li> </ul>

Table 3: Numerical protocol for Fluent airfoil study

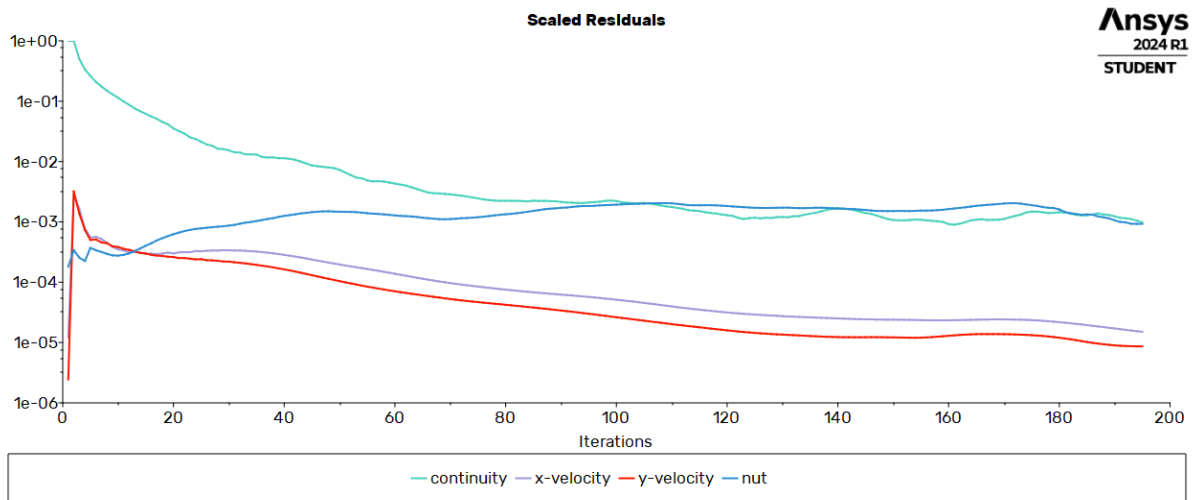


Figure 17: Residuals of the simulation as a function of the number of iterations for an angle of incidence of  $12^\circ$

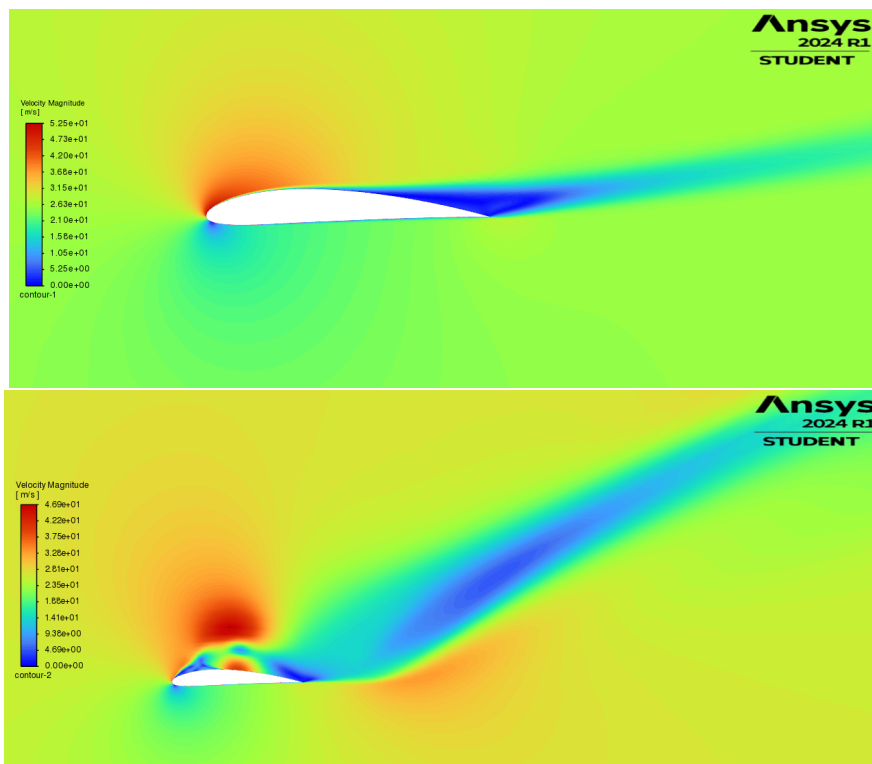


Figure 18: Speed contours for wing incidence angles of  $12^\circ$  (top) and  $20^\circ$  (bottom). It can be seen that the air wake covers a larger area when the wing angle of incidence increases.

### A.6 Other figures

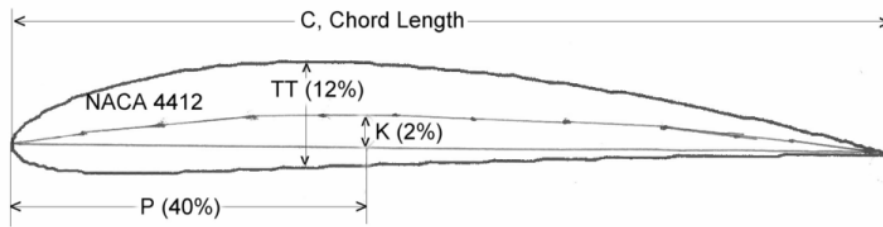


Figure 19: Diagram of the NACA4412 airfoil profile [10]

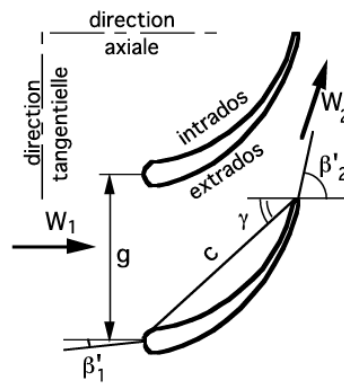


Figure 20: Diagram of the blade profile used [4]

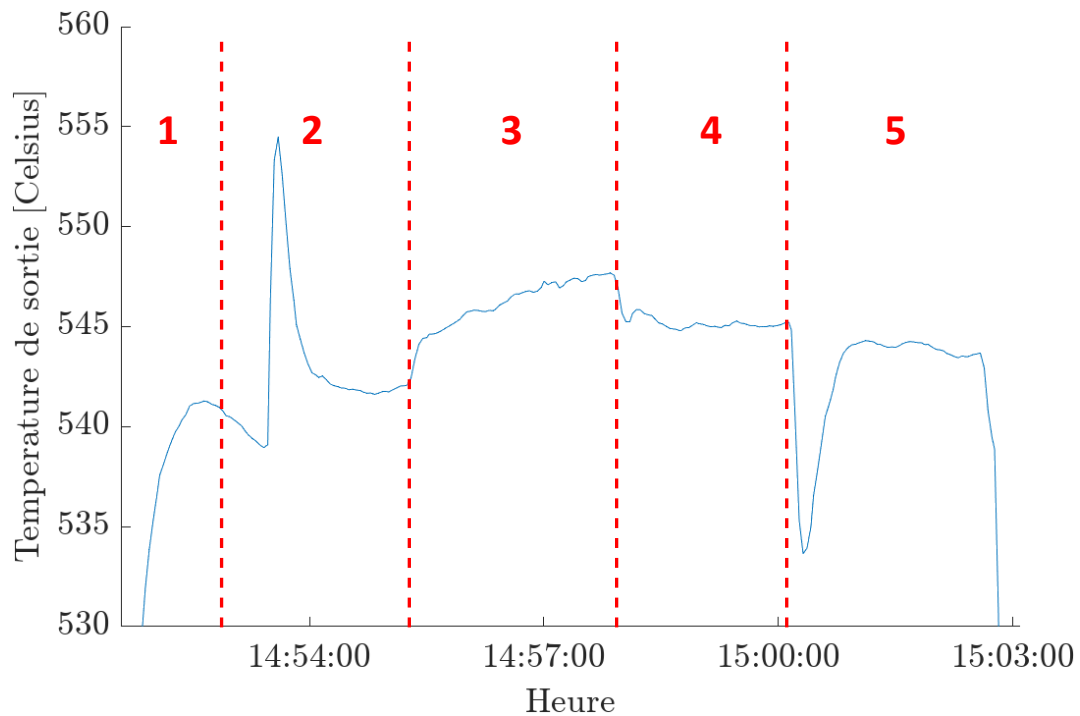


Figure 21: Reactor outlet temperature as a function of time. Sequence of kerosene flow "low(1), medium(2), high(3), medium(4), low(5)".

## A.7 Programs *Matlab* used

Listing 1: Matlab code for calculating momentum on the blade grid

```

1 % Calcul de la force exercee sur l'aube de la grille d'aubes
2 % l'aide de l'equation de quantite de mouvement
3
4 % IMPORTATION DES DONNEES
5
6 SP_V10 = readtable('data/sonde proche vitesse max.csv');
7 SP_V5 = readtable('data/vitesse 5 sonde proche.csv');
8
9
10 % DONNEES
11
12 % Pas de l'aube
13 PasAube = 0.100; % (en m)
14
15 % Corde
16 Corde = 0.128;% (en m)
17
18 % Viscosite de l'air
19 nu = 0.000015;

```

```

20
21 % Pression et temperature atmospheriques mesurees
22 PatmmHg = 742; % (en mm Hg) le 31/05
23 TatmCelsius = 24; % (en degres Celsius) le 31/05
24
25 % Calcul de la pression atmospherique
26 Patm = 13.6*9.81*PatmmHg; % (en Pascals)
27 % Calcul de la masse volumique de l'air
28 rho = Patm/(287*(273.15 + TatmCelsius)); % (en Kg/m3)
29
30 % valeur du potentiometre
31 potentiometre = 5
32
33 if potentiometre == 10
34     % Sonde amont
35     ptotamont = 343 + Patm; % (en Pascals) le 31/05  vitesse max
36     psamont = 323 + Patm; % en Pa  vitesse max
37     pdynamont = ptotamont - psamont; % (en Pa)
38     % Sonde lointaine
39     ptot3 = 251 + Patm;
40     pdyn3 = ptot3 - 41;
41     BetaAval3 = 72.5; % angle en degrs
42     % Sonde proche
43     SP = SP_V10; % Prendre uniquement le deuxime tableau
44 else
45     % Sonde amont
46     ptotamont = 94 + Patm; % (en Pascals) le 31/05  vitesse max
47     psamont = 90 + Patm; % en Pa  vitesse max
48     pdynamont = ptotamont - psamont; % (en Pa)
49     % Sonde lointaine
50     ptot3 = 251 + Patm;
51     pdyn3 = ptot3 - 41;
52     BetaAval3 = 72.5; % angle en degrs
53     % Sonde proche
54     SP = SP_V5; % Prendre uniquement le deuxime tableau
55 end
56
57 %pdynamont = ptotamont - psamont; % (en Pa)
58 Vamont = sqrt(2*pdynamont/rho) % (en m/s)
59
60 % Calcul du debit massique par unite de largeur
61 mpoint = rho * Vamont * PasAube; % (en Kg/s /unite de largeur)
62
63 % Donnees a l'aval proche
64 z = SP.z/1000; % altitude (en m)
65 ptotaval = SP.PressionTotaleSondeProche + Patm;% avec etalonnage de la
    sonde (en Pascals)

```

```

66 pdynaval = ptotaval - (SP.PressionGaucheSondeProche + Patm); % avec
    etalonnage de la sonde (en Pascals)
67 Beta = SP.alpha*2*pi/360; % Angle (en radians)
68 Vaval = sqrt(2*pdynaval/rho); % vitesse axiale (en m/s)
69 Vavalx = Vaval.*cos(Beta); % composante x
70 Vaval y = Vaval.*sin(Beta); % composante y
71
72 % Calcul des grandeurs moyennes aval proche
73 Vavalxmy = trapz (z,Vavalx)/abs(z(1)-z(size(z,1)));
74 Vavalymy = trapz (z,Vaval y)/abs(z(1)-z(size(z,1)));
75 Vavalmy = trapz (z,Vaval)/abs(z(1)-z(size(z,1)))
76 BetaAvalmy = atan(Vavalymy/Vavalxmy);
77 BetaAvalmyDeg = BetaAvalmy*180/pi
78 Betamy = atan(tan(BetaAvalmy)/2); % Angle moyen entre sortie
79
80 % Calcul des pressions totale et dynamique, vitesse aval lointain
81 %ptot3 = 1000*9.81*0.01*ptot3cmH2O*CoeffPtot3 + Patm; % (en Pascals)
82 %pdyn3 = 1000*9.81*0.01*pdyn3cmH2O*CoeffPdyn3; % (en Pascals)
83 V3 = sqrt(2*pdyn3/rho) % (en m/s)
84 V3x = V3*cos(BetaAval3*pi/180); % composante x
85 V3y = V3*sin(BetaAval3*pi/180); % composante y
86
87 % Calcul de Fx et Fy a partir des donnees amont et aval proche
88 A = rho*trapz(z,Vavalx.*Vavalx); % Calcul de l'integrale rho V2x*V2x ds
89 B = trapz(z,ptotaval-pdynaval); % Calcul de l'integrale de p2 ds
90 C = rho * trapz(z, Vavalx.*Vaval y); % Calcul de l'integrale de rho V2x*
    V2y ds
91 D=0; % Calcul de l'integrale de tau2xx ds
92 E=0; % Calcul de l'integrale de tau2xy ds
93 Fx2 = mpoint * Vamont - A + (ptotamont-pdynamont) * PasAube - B + D
94 Fy2 = - C + E
95
96 % Calcul de Fx et Fy a partir des donnees amont et aval lointain
97 Fx3 = mpoint * (Vamont - V3x) + ((ptotamont-pdynamont)-(ptot3-pdyn3)) *
    PasAube
98 Fy3 = - mpoint * V3y
99
100 % Calcul des coefficients de portance et de trainee
101 Cx2 = 2*Fx2 / (rho*Corde*Vavalmy^2);
102 Cy2 = 2*Fy2 / (rho*Corde*Vavalmy^2);
103 CL2 = - Cx2*sin(Betamy)+Cy2*cos(Betamy) % Portance
104 CD2 = Cx2*cos(Betamy)+Cy2*sin(Betamy) % Trainee
105 Cx3 = 2*Fx3 / (rho*Corde*Vavalmy^2);
106 Cy3 = 2*Fy3 / (rho*Corde*Vavalmy^2);
107 CL3 = - Cx3*sin(Betamy)+Cy3*cos(Betamy) % Portance
108 CD3 = Cx3*cos(Betamy)+Cy3*sin(Betamy) % Trainee
109

```

```

110
111 % TRACE DES COURBES
112
113 % Repartition des pressions totales aval proche
114 ptotaval=ptotaval-Patm;
115
116 hfig = figure; % save the figure handle in a variable
117 plot(z, ptotaval, 'ob-', 'LineWidth',1.5);
118 xlabel('$z$ (m)');
119 ylabel('$p_{tot} - p_{atm}$ (Pa)');
120 fname = 'pression_tot_aval';
121
122 picturewidth = 20; % set this parameter and keep it forever
123 hw_ratio = 0.65; % feel free to play with this ratio
124 set(findall(hfig, '-property', 'FontSize'), 'FontSize', 17) % adjust
    fontsize to your document
125
126 set(findall(hfig, '-property', 'Box'), 'Box', 'off') % optional
127 set(findall(hfig, '-property', 'Interpreter'), 'Interpreter', 'latex')
128 set(findall(hfig, '-property', 'TickLabelInterpreter'), '
    TickLabelInterpreter', 'latex')
129 set(hfig, 'Units', 'centimeters', 'Position', [3 3 picturewidth hw_ratio*
    picturewidth])
130 pos = get(hfig, 'Position');
131 set(hfig, 'PaperPositionMode', 'Auto', 'PaperUnits', 'centimeters', '
    PaperSize', [pos(3), pos(4)])
132 print(hfig, fname, '-dpdf', '-vector', '-fillpage')
133
134
135 % Repartition des angles aval proche
136 Beta=Beta*180.0/pi;
137
138 plot(z, Beta, 'ob-', 'LineWidth',1.5);
139 xlabel('$z$ (m)');
140 ylabel('$\beta$ (deg)');
141 fname = 'angle_ecoulement';
142
143 picturewidth = 20; % set this parameter and keep it forever
144 hw_ratio = 0.65; % feel free to play with this ratio
145 set(findall(hfig, '-property', 'FontSize'), 'FontSize', 17) % adjust
    fontsize to your document
146
147 set(findall(hfig, '-property', 'Box'), 'Box', 'off') % optional
148 set(findall(hfig, '-property', 'Interpreter'), 'Interpreter', 'latex')
149 set(findall(hfig, '-property', 'TickLabelInterpreter'), '
    TickLabelInterpreter', 'latex')

```

```
150 set(hfig, 'Units', 'centimeters', 'Position', [3 3 picturewidth hw_ratio*  
    picturewidth])  
151 pos = get(hfig, 'Position');  
152 set(hfig, 'PaperPositionMode', 'Auto', 'PaperUnits', 'centimeters', '  
    PaperSize', [pos(3), pos(4)])  
153 print(hfig, fname, '-dpdf', '-vector', '-fillpage')
```

Listing 2: Matlab code for blade profile pressure integration

```

1 %%%%%%%%%% DONNEES %%%%%%%%%%
2
3 % Corde
4 Corde = 0.128; % (en m)
5
6 % Chargement des valeurs des pressions sur l'aube (en cm H2O)
7 NbPoints = 36;
8
9 % Pression et temperature atmospheriques mesurees
10 PatmmHg = 742; % (en mm Hg) le 31/05
11 TatmCelsius = 24; % (en degres Celsius) le 31/05
12
13 % Calcul de la pression atmospherique en Pascals
14 Patm = 13.6*1000*9.81*0.001*PatmmHg;
15
16 % Lecture des coordonnees des aubes en position calee
17 load aube1calee.dat;
18 x = aube1calee(:,1); % axe horizontal vers l'aval (en m)
19 y = aube1calee(:,2); % axe vertical vers le bas (en m)
20 xbf = 0.078; % coordonnees du bord de fuite
21 ybf = 0.102;
22
23 % Vitesse et angle moyens aval issus du calcul QuantiteMouvement
24
25 potentiometre = 10; % valeur du potentiometre pour le choix des dbits
26
27 if potentiometre == 10
28     Vavalmy = 26.7400; % (en m/s)
29     BetaAvalmy = 79.7042*pi/180; % (en radians)
30     p1 = Pstat_aube_V10_V5(1,4:end)';
31
32 else
33     Vavalmy = 14.0712; % (en m/s) le 31/05
34     BetaAvalmy = 79.6870*pi/180;% (en radians) le 31/05
35     p1 = Pstat_aube_V10_V5(2,4:end)';
36 end
37
38 % Calcul de la masse volumique
39 rho = Patm/(287*(273+TatmCelsius)); % (en Kg/m3)
40
41 % Coordonnees de l'aube sur un repere qui lui est lie
42 y = -y; % Remet l'axe vertical vers le haut (pour le trace)
43 calage1 = 53; % Angle de calage de l'aube (en degres)
44 calage1 = calage1*2*pi/360;
45 x1 = x*cos(calage1)+y*sin(calage1); % positif du BA vers de BF
46 y1 = -x*sin(calage1)+y*cos(calage1); % positif de l'extrados vers l'

```

```

    intrados
47
48 % Calcul des composantes des vecteurs normaux a chacun des segments du
49 % profil d'aube
50 nx = -y(1:NbPoints-1) + y(2:NbPoints);
51 ny = x(1:NbPoints-1) - x(2:NbPoints);
52 mod = sqrt(nx.^2 + ny.^2);
53 nx = nx ./ mod;
54 ny = ny ./ mod;
55
56 nx0 = +y(1) - ybf; % calcul de la premiere normale
57 ny0 = -x(1) + xbf;
58 mod0 = sqrt(nx0.^2 + ny0.^2);
59 nx0 = nx0 / mod0;
60 ny0 = ny0 / mod0;
61 nx = [nx' nx0]';
62 ny = [ny' ny0]';
63 mod = [mod' mod0]';
64 clear nx0 ny0 mod0;
65
66 nx0 = -y(NbPoints) + ybf; % calcul de la derniere normale
67 ny0 = +x(NbPoints) - xbf;
68 mod0 = sqrt(nx0.^2 + ny0.^2);
69 nx0 = nx0 / mod0;
70 ny0 = ny0 / mod0;
71 nx = [nx' nx0]';
72 ny = [ny' ny0]';
73 mod = [mod' mod0]';
74 clear nx0 ny0 mod0;
75
76 % Calcul des points au centre des segments du profil d'aube
77 X = (x(1:NbPoints-1) + x(2:NbPoints)) / 2.;
78 Y = (y(1:NbPoints-1) + y(2:NbPoints)) / 2.;
79
80 X0 = (x(1) + xbf) / 2.; % premier segment
81 Y0 = (y(1) + ybf) / 2.;
82 X = [X' X0]';
83 Y = [Y' Y0]';
84 clear X0 Y0;
85
86 X0 = (xbf + x(NbPoints)) / 2.; % dernier segment
87 Y0 = (ybf + y(NbPoints)) / 2.;
88 X = [X' X0]';
89 Y = [Y' Y0]';
90 clear X0 Y0;
91
92 % Calcul des pressions moyennes sur les centres des segments du profils

```

```

93 % d'aube
94 p = p1; % (en Pascals)
95 P = (p(1:NbPoints-1) + p(2:NbPoints)) / 2.;
96
97 P0 = p(1); % pression sur le premier segment
98 P = [P' P0]';
99 clear P0;
100 P0 = p(NbPoints); % pression sur le dernier segment
101 P = [P' P0]';
102 clear P0;
103
104 % Calcul des composantes de la force s'exercant sur chaque segment
105 fx = -P .* nx .* mod; % ici mod = ds
106 fy = -P .* ny .* mod; % ici mod = ds
107
108 % Calcul des composantes de la force qui s'exerce sur l'aube
109 Fx = sum(-P .* nx .* mod)% (en N)
110 Fy = sum(-P .* ny .* mod)% (en N)
111
112 % Calcul des coefficients de portance et de trainee
113 Cx = 2*Fx / (rho*Corde*Vavalmy^2);
114 Cy = 2*Fy / (rho*Corde*Vavalmy^2);
115 Betamy = atan(tan(BetaAvalmy)/2);
116 CL = - Cx*sin(Betamy)+Cy*cos(Betamy)
117 CD = Cx*cos(Betamy)+Cy*sin(Betamy)
118
119 % TRACE DES COURBES
120
121 % Comparaison des profils adimensionnes
122
123 V_ament_V10 = 5.8702;
124 Vavalmy_V10 = 26.7400;
125 p_V10 = Pstat_aube_V10_V5(1,4:end)'; %pstataile-patm
126 ptot_ament_V10 = 343; %ptot-patm
127 pstat_ament_V10 = 323;%pstatament-patm
128 Cp_V10 = (p_V10-pstat_ament_V10)/(rho*V_ament_V10^2/2);
129
130 Vavalmy_V5 = 14.0712;
131 V_ament_V5 = 2.6252;
132 p_V5 = Pstat_aube_V10_V5(2,4:end)';
133 ptot_ament_V5 = 94;
134 pstat_ament_V5 = 90;
135 Cp_V5 = (p_V5-pstat_ament_V5)/(rho*V_ament_V5^2/2);
136
137 figure,
138 plot(x1,Cp_V10,'b+',DisplayName='$C_P^{10}$')
139 hold on

```

```

140 plot(x1,Cp_V5,'rx',DisplayName='$C_P^{5}$')
141 hold off
142 grid on;
143 legend({'$C_P^{10}$', '$C_P^{5}$'}, Interpreter="latex");
144 xlabel('$x$ (m)', Interpreter='latex');
145 ylabel('$C_p$',Interpreter='latex');
146
147 % Repartition des pressions sur l'aube
148 figure;
149 hold on;
150 plot(x1, p, 'ob-');
151 grid on;
152 legend('Pression sur le profil');
153 xlabel('x1 (m)');
154 ylabel('Ps - Patm (Pa)');
155
156 % Dessin de l'aubage
157 figure;
158 hold on;
159 xdessin = [x' xbf]';
160 ydessin = [y' ybf]';
161 xdessin = [xdessin' x(1)]';
162 ydessin = [ydessin' y(1)]';
163 plot(xdessin,ydessin, '+-')
164 axis([-0.03 0.1 -0.020 0.110]);
165 xlabel('x (m)');
166 ylabel('z (m)');
167 axis square;
168
169 % Repartition des vecteurs forces de pression sur l'aube
170 quiver(X, Y, fx, fy, 'k');
171 grid;

```

Listing 3: Matlab code for calculating thrust force in turbojet

```

1
2 table=readtable('theme12-070624pm.txt')
3
4 egt=table.EGT;
5 time=table.Time;
6
7 hfig=figure;
8 plot(time,egt)
9 ylim([530,560])
10 xlabel('Heure')
11 ylabel('Temperature de sortie [Celsius]')
12 picturewidth = 20; % set this parameter and keep it forever
13 hw_ratio = 0.65; % feel free to play with this ratio
14 set(findall(hfig,'-property','FontSize'),'FontSize',17) % adjust
    fontsize to your document
15 set(findall(hfig,'-property','Box'),'Box','off') % optional
16 set(findall(hfig,'-property','Interpreter'),'Interpreter','latex')
17 set(findall(hfig,'-property','TickLabelInterpreter'),'
    TickLabelInterpreter','latex')
18 set(hfig,'Units','centimeters','Position',[3 3 picturewidth hw_ratio*
    picturewidth])
19 pos = get(hfig,'Position');
20 set(hfig,'PaperPositionMode','Auto','PaperUnits','centimeters','
    PaperSize',[pos(3), pos(4)])
21
22
23 %1:14h52:42
24 %2:14h54:47
25 %3:14h57:54
26 %2:14h59:39
27 %1:15h01:55
28
29 durees=['14:52:42';'14:54:47';'14:57:54';'14:59:39';'15:01:55'];
30
31 cpa=1004; %capacite calorifique massique air
32 cpg=1147; %capacite calorifique massique gaz brules
33 cp=(cpa+cpg)/2; %moyenne
34 ga=1.4; %gamma air
35 gg=4/3; %gamma gaz brules
36 g=(ga+gg)/2; %moyenne
37 ra=(ga-1)/ga*cpa;% r air
38 rg=(gg-1)/gg*cpg;% r gaz brules
39 r=(ra+rg)/2; %moyenne
40
41 Tsalle=25+273.15; %en K
42 Psalle=747;% en mmMercure

```

```

43 patm=Psalle*133.322387415; % en Pa
44 rho=patm/ra/Tsalle; %masse volumique de l'air dans la salle
45
46 D5=0.05587; %diamtre sortie (en m)
47 A5=pi/4*D5^2; %section de sortie
48
49 %Traitement :
50
51 for i=1:5
52
53 %Rcupration donnees:
54 valeurRecherchee = duration(durees(i,:));
55 indexLigne = find(table.Time == valeurRecherchee);
56 % Rcuprer la ligne
57 ligne = table(indexLigne,:);
58 ligne.Time;
59
60
61 %Point 1
62 T01=ligne.CompInlet+273.15; %T direct en K
63 Pdyn1=ligne.CompInletPress; %P dynamique en PSI
64 Pdyn1=Pdyn1*0.06894753e5;%P dynamique en Pa
65 P01=patm;% P tot
66
67
68 %Point 2
69 T02=ligne.CompExitTemp+273.15; %T direct en K
70 P02=ligne.CompExitPress; %P tot en PSIG
71 P02=P02*0.06894753e5+patm;%P tot en Pa
72
73 %Point 3
74 T03=ligne.TurbInletTemp+273.15; %T direct en celsius
75 P03=ligne.TurbInletPress; %P tot en PSIG
76 P03=P03*0.06894753e5+patm;%P tot en Pa
77
78 %Point 4
79 T04=ligne.TurbExitTemp+273.15; %T direct en celsius
80 P04=ligne.TurbExitPress; %P tot en PSIG
81 P04=P04*0.06894753e5+patm;%P tot en Pa
82
83
84 %Point 5
85 T05=ligne.EGT+273.15; %T direct en celsius
86 P05=ligne.NossExitPress; %P tot en PSIG
87 P05=P05*0.06894753e5+patm;%P tot en Pa
88
89

```

```
90
91
92 %Calcul de la force de pousse
93 T5=T05*(patm/P05)^((g-1)/g); %température statique
94 rho5=patm/(r*T5); %masse volumique en sortie
95
96
97 %a partir de la mesure
98 Fexp=ligne.Thrust*0.45359*9.81; %lbs to N
99 %attention a retirer l'offset :
100 Fexp=Fexp-(3.0850*0.45359*9.81);
101
102 %a partir de la formule theorique
103 u5=sqrt(2*cp*(T05-T5)); %vitesse en sortie
104 mpoint5=rho5*A5*u5; %debit massique en sortie
105 Fthe5=mpoint5*u5; %force de poussee en sortie
106
107 disp(["Debit d'air en sortie",num2str(mpoint5)])
108 disp(['Force de pousse thorique ',num2str(Fthe5),'N']);
109 disp(['Force de pousse exprimentale ',num2str(Fexp),'N']);
110 end
```